Asociación Argentina
de Mecánica Computacional

Mecánica Computacional Vol XXIX, págs. 9855-9868 (artículo completo)
Eduardo Dvorkin, Marcela Goldschmit, Mario Storti (Eds.)
Buenos Aires, Argentina, 15-18 Noviembre 2010

# NUMERICAL SIMULATION OF REINFORCED CONCRETE STRUCTURES USING A MULTIPHASE APPROACH AND A PLASTICITY-BASED SMEARED CRACK MODEL

**Marcelo P. Figueiredo , Samir Maghous , Américo Campos Filho**

[a]*PPGEC-UFRGS, Av. Osvaldo Aranha, 99, 3° andar-90035-190, Porto Alegre, RS, Brasil, marcelo.porto@ufrgs.br, http://www.ppgec.ufrgs.br/*

**Keywords:** Multiphase model, Homogenization, Finite Element Method.

**Abstract**. Assessing the global behavior of reinforced materials from the individual properties of their components has been the subject of a considerable amount of experimental and theoretical works in the last years. The so-called multiphase model is an alternative generalization of the homogenization method and it relies upon the idea that, at the macroscopic scale, the reinforced concrete is a geometrical superposition of the matrix phase (concrete) and the reinforcing phase (steel bars). The constitutive equations for the homogenized reinforced concrete structures are formulated and the corresponding numerical implementation is described. Considering the particular case of concrete structures, Figueiredo et al. (2009) analyzed the mechanical behavior of reinforced concrete flat slabs under prescribed loading using an elastoplastic multiphase model. The present contribution extends the previous numerical code to account for concrete cracking by implementing the smeared crack model presented by Hinton (1988). As expected, the numerical implementation with multiphase approach leads to a significantly reduced computational time with respect to a direct numerical simulation in which the steel bars are treated as individual structural elements embedded in the concrete matrix. (FIGUEIREDO et al., Elastoplastic multiphase model for reinforced concrete flat slabs, In: *XXX CILAMCE*, 2009; HINTON, E., *Numerical methods and software for dynamic analysis of plates and shells*, 1988).

## 1 INTRODUCTION

The capacity of predicting the essential characteristics that govern the behavior of materials reinforced by stiff linear inclusions from the properties of the individual components still remains a major concern in structural engineering of composite materials, and a significant number of works has been dedicated to this subject in the last decades.

As far as the finite element modeling of reinforced concrete structures is concerned, steel bars are traditionally accounted for through three ways (CEB, 1983): 1) by means of a continuous equivalent model as often used in the case of plates and shells, substituting the dense reinforcement by equivalent layers, 2) through a discrete modeling in which the steel bars are represented by one-dimensional elements frequently associated with appropriate adherence elements, and 3) through the so-called "embedded model" where each bar is considered as a stiffer linear inclusion embedded within the element of concrete matrix, thus resulting in an element stiffness equal to the sum of concrete matrix and steel bar contribution. However such approaches can come up against serious numerical difficulties when the number of bars involved in the structure becomes higher. Indeed, the computational cost may eventually be prohibitively large since three-dimensional analysis is generally needed to take into account interactions between concrete matrix and inclusions properly and since non-linear constitutive models, such as plasticity, have to be utilized in order to obtain relevant results.

An alternative approach called multiphase model was recently developed, providing a mechanically consistent framework to analyze the behavior of structures made up of materials reinforced by linear continuous inclusions. The general formulation of the model is presented in Sudret (1999) together with applications in the field of geotechnical engineering. Extensions of the multiphase model have been introduced by Bennis (2002) and later by Hassen (2006). The method has been applied to a large variety of problems involving reinforced soils such as reinforced earth, micropile networks and rock-bolted tunnels may be found in de Buhan and Sudret (1999, 2000, 2001) or Hassen and de Buhan (2005, 2006). The main advantage of such modeling lies in a significantly reduced computational effort, compared to that required in direct numerical simulations.

## 2 THE MULTIPHASE MODEL FOR REINFORCED CONCRETE

### 2.1 Description of the model

Considering the reinforced concrete as a matrix of concrete with steel bars arranged periodically (Figure 1). The typical size of the structure being significantly greater than the diameter of the inclusions and their spacing. Consider the reinforced concrete as homogenous medium.

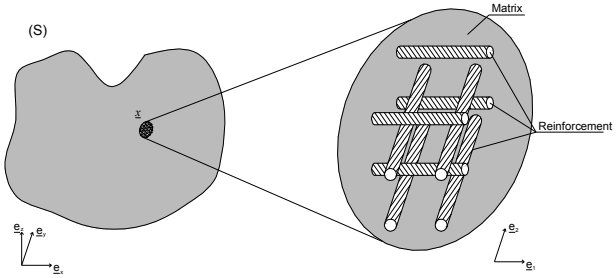


Figure 1 – Description of the reinforced material, Hassen (2006).

Sudret (1999) explains that to any point of a volume Ω of reinforced material are associated geometrically coincident particles: one particle of the matrix phase and N particles of the reinforcement phase. These N + 1 superposed particles form the multiphase medium.

$$d\Omega(\underline{x}) = d\Omega^m(\underline{x}) \bigcup_{r=1,...N} d\Omega^r(\underline{x}) \tag{1}$$

In this way, the steel bars are grouped in a finite number of N different families, each one of these families characterized by a direction given by a unit vector er (r = 1, ..., N). The number of reinforcement families will be the same to the number of directions in which the bars are disposed.

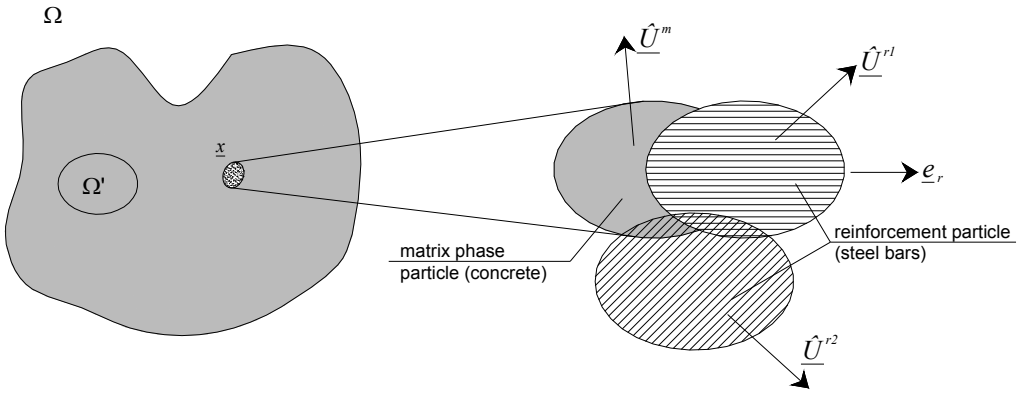


Figure 2 – Description of the material with the matrix phase and two reinforcement phases.

## 2.2 Efforts behaviour

The matrix phase is modelled as Cauchy continuum. It can be shown that the internal forces are described by a second-order symmetrical tensor denoted by $\underline{\underline{\sigma}}^m$. This quantity will be referred to as the matrix phase stress tensor.

It is admitted that the inclusions are assumed to take only tensile-compressive forces, that is, shear forces and bending moments are disregarded, Hassen (2006) applies the multiphase model taking into account that the inclusions takes these efforts. So, the variable that describes the internal forces in the reinforcement phase turns out to be a scalar stress, noted $\sigma^r$.

Finally, due to the superposition of N+1 particles in each point, body forces, $I^j$, are introduced to account for the interaction between phases.

The external forces applied onto a geometrical volume Ω are prescribed in each phase j separately, and consists in:

(a) Body forces denoted by $\rho^j \underline{F}^j$ (gravity) exerted by the outside of Ω.

(b) Tractions $\underline{T}^j$ applied at the boundary $\partial\Omega$.

The inertial forces are computed by means of the phase acceleration fields denoted by $\underline{\gamma}^j$.

### 2.3 Equations of motion

In this way, the equations of motion of the multiphase model are given, in agreement with Sudret (1999), for each phase separately as follows.

$$div\underline{\underline{\sigma}}^{m}(\underline{x})+\rho^{m}(\underline{x})(F^{m}(\underline{x})-\gamma^{m}(\underline{x}))+\sum_{r=1}^{\mathbf{N}}\underline{I}^{r}(\underline{x})=0 \tag{2}$$

$$div\left(\sigma^{r}(\underline{x})\underline{e}_{r}\otimes\underline{e}_{r}\right)+\rho^{r}(\underline{x})(F^{r}(\underline{x})-\gamma^{r}(\underline{x}))-\underline{I}^{r}(\underline{x})=0,\quad r=1,...N \tag{3}$$

The corresponding boundary conditions are

$$\underline{T}^{m}(\underline{x})=\underline{\underline{\sigma}}^{m}(\underline{x})\cdot\underline{n}(\underline{x}) \tag{4}$$

$$\underline{T}^{r}(\underline{x})=\sigma^{r}(\underline{x})\left(\underline{n}(\underline{x})\cdot\underline{e}_{r}\right)\underline{e}_{r},\quad r=1,...N \tag{5}$$

Equations (2) and (4) are the equations of motion of a Cauchy continuum, where the interaction forces appear as body forces. These interaction forces reveal, at the macroscopic scale, the interface forces between each inclusion and the surrounding matrix at the microscopic scale, and can thus be interpreted as the average of the latter on a unit volume.

### 2.4 Perfect bonding model

Sudret (1999) and de Buhan and Sudret (2001) present a particular case of the two-phase model where is admitted the perfect bonding hypothesis: all phases have the same displacement field. This model is going to allow to treat problems of reinforced concrete in what is supposed to be no slippage between the steel bars and the concrete matrix. So:

$$\underline{\xi}^{m}=\underline{\xi}^{r}\equiv\underline{\xi} \tag{6}$$

Taking into account the perfect bonding hypothesis, is introduced, with no ambiguity, the total strain tensor:

$$\underline{\underline{\in}}=\frac{1}{2}\left(\underline{\underline{grad\,\xi}}+{}^{t}\underline{\underline{grad\,\xi}}\right) \tag{7}$$

The compatibility equations between the phase strain variables are:

$$\underline{\underline{\varepsilon}}^{m}=\underline{\underline{\in}};\quad \varepsilon^{r}=\underline{\underline{\in}}:\left(\underline{e}_{r}\otimes\underline{e}_{r}\right)\equiv\in_{rr} \tag{8}$$

In this model, the system kinematics is described by a single displacement field $\xi$. Bennis (2002) carries out the application of the model to geotechnical structures taking into account the interaction matrix/reinforcement.

It is thus relevant do derive global equations of motion for the whole system. These equations are obtained by summing up Eq. (2), (3) and the Eq. (4), (5) respectively. Introducing the following notation:

$$\rho \underline{F} = \sum_j \rho^j \underline{F}^j \;\; ; \;\; \underline{T} = \sum_j \underline{T}^j \;\; ; \;\; \rho \underline{\gamma} = \sum_j \rho^j \underline{\gamma}^j \tag{9}$$

$$\underline{\underline{\Sigma}} = \underline{\underline{\sigma}}^m + \sum_{r=1}^{N} \sigma^r \underline{e}_r \otimes \underline{e}_r \tag{10}$$

with $j \in \{m, r = 1,...N\}$, one gets:

$$div \; \underline{\underline{\Sigma}} + \rho \left( \underline{F} - \underline{\gamma} \right) = \underline{0} \tag{11}$$

$$\underline{T} = \underline{\underline{\Sigma}} \cdot \underline{n} \tag{12}$$

The tensor of total stress $\underline{\underline{\Sigma}}$ appears to be the sum of the partial tensor in the matrix phase and the uniaxial partial stress tensor in the reinforcement phase. With this notation, the constitutive Eq. (11) and (12) reduce to those of the classical Cauchy continuum.

To complete the description of the perfect bonding model, global constitutive equation relating $\underline{\underline{\Sigma}}$ and $\underline{\underline{\in}}$ are derived. One can easily prove that the global tensor of elastic moduli $\underline{\underline{\underline{\underline{A}}}}$ satisfying $\underline{\underline{\Sigma}} = \underline{\underline{\underline{\underline{A}}}} : \underline{\underline{\in}}$ in the elastic domain write:

$$\underline{\underline{\underline{\underline{A}}}} = \underline{\underline{\underline{\underline{a}}}}^m + \sum_{r=1}^{N} a^r \underline{e}_r \otimes \underline{e}_r \otimes \underline{e}_r \otimes \underline{e}_r \tag{13}$$

where the global tensor of elastic moduli is decomposed additively in a contribution of the matrix phase and a contribution of each reinforcement phase. It appears clearly that the directions $\underline{e}_r$ are privileged, what is seen in the anisotropic characteristic of the behavior.

Equilibrium equations and constitutive laws have been derived, making it possible to solve boundary value problems. In order to model real reinforced structures, it is now necessary to connect the phase constitutive laws with the material characteristics of the concrete and inclusions.

de Buhan and Sudret (2001) assumed that the volume fraction $\eta^r$ of the inclusion is small compared to one:

- The matrix phase constitutive law is identified with that of the concrete.
- Supposing that the inclusions take axial force only it is possible to calculate the reinforcement phase stiffness as:

$$a^r = \eta^r \cdot E^{inc} \tag{14}$$

where $E^{inc}$ is the Young's modulus of the steel bars.

## 3 NUMERICAL IMPLEMENTATION OF THE MODEL

The implementation formulated here follows the steps presented by Sudret (1999), Hassen (2006) and de Buhan and Sudret (2001).

### 3.1 Description of the model

In case of perfect bonding, considering a kinematically admissible virtual displacemente field $\hat{\underline{\xi}}$ and its associated linear strain field $\hat{\underline{\underline{\varepsilon}}}$, the principle of virtual work, derived from (11) and (12), satisfies:

$$\int_{\Omega} \underline{\underline{\Sigma}} : \underline{\underline{\hat{\varepsilon}}}\, d\Omega - \int_{\Omega} \rho F \cdot \underline{\hat{\xi}}\, d\Omega - \int_{\partial\Omega} \underline{T}^{d} \cdot \underline{\hat{\xi}}\, dS = 0 \tag{15}$$

Relating the elastic strain to the phase stress by $\underline{\underline{\sigma}}^{m} = \underline{\underline{\underline{\underline{a}}}}^{m} : \left(\underline{\underline{\varepsilon}}^{m} - \underline{\underline{\varepsilon}}_{p}^{m}\right)$ and $\sigma^{r} = a^{r}\left(\varepsilon^{r} - \varepsilon_{p}^{r}\right)$ and substituting in Eq. (11) and using the Eq. (8), the first term in Eq. (15) may be rewritten as follows:

$$\int_{\Omega} \underline{\underline{\Sigma}} : \underline{\underline{\hat{\varepsilon}}}\, d\Omega = \int_{\Omega} \left[ \underline{\underline{\underline{\underline{A}}}} : \underline{\underline{\varepsilon}} - \underline{\underline{\underline{\underline{a}}}}^{m} : \underline{\underline{\varepsilon}}_{p}^{m} - a^{r} \varepsilon_{p}^{r} \underline{e}_{r} \otimes \underline{e}_{r} \right] : \underline{\underline{\hat{\varepsilon}}}\, d\Omega \tag{16}$$

The geometric volume is discretized into $N_e$ elements. The displacement field $\underline{\xi}$ in each element $\nu^e$ is approximated as follows

$$\forall x \in \nu^{e},\ \xi(x)_{|\nu^e} = \mathrm{N}_{e}(\underline{x}) \cdot \underline{u}_{e} \tag{17}$$

where $\underline{u}_e$ is the vector of element nodal displacements and $\mathbf{N}_e(\underline{x})$ are the shape functions. The strain vector is classically given by:

$$\underline{\varepsilon} = \mathbf{B}_{e}(\underline{x}) \cdot \underline{u}_{e} \tag{18}$$

where the matrix $\mathbf{B}_e$ contains partial derivatives of the shape functions with respect to the coordinates. Consequently, the matrix phase stress vector is:

$$\underline{\sigma}^{m} = \mathbf{d}^{m} \cdot \left(\underline{\varepsilon} - \underline{\varepsilon}_{p}^{m}\right) \tag{19}$$

It is introduced now an additional notation for dealing with the reinforcement phase. Let us denote by $\underline{\mathbf{e}}_{\mathbf{r}}$ the vector of the six components of $\underline{e}_r \otimes \underline{e}_r$. The compatibility Eq. (7) can be rewritten as:

$$\varepsilon^{r} = {}^{t}\underline{\mathbf{e}}_{\mathbf{r}} \cdot \underline{\varepsilon} = {}^{t}\underline{\varepsilon} \cdot \underline{\mathbf{e}}_{\mathbf{r}} \tag{20}$$

Substituting the above equations in the principle of virtual work (15) and using (16), one gets the discretized formulation, which leads to the usual linear system yielding the global vector of nodal displacement $\underline{U}$.

$$\mathbf{K} \cdot \underline{U} = \underline{F}^{ext} + \underline{F}_{p}^{m} + \underline{F}_{p}^{r} \tag{21}$$

The global stiffness matrix **K** turns out to be:

$$\mathbf{K} = \sum \int_{\nu^e} {}^{t}\mathbf{B}_{e} \left( \mathbf{d}^{m} + \sum_{r=1}^{N} a^{r}\, \underline{\mathbf{e}}_{\mathbf{r}} \cdot {}^{t}\underline{\mathbf{e}}_{\mathbf{r}} \right) \mathbf{B}_{e}\, d\nu^{e} \tag{22}$$

the terms in the right-hand side of Eq. (33) are the external load vector:

$$F^{ext} = \sum \left( \int_{\nu^e} {}^{t}\mathbf{N}_{e} \cdot \underline{\rho F}\, d\nu^{e} + \int_{\partial\Omega \cap \nu^e} {}^{t}\mathbf{N}_{e} \cdot \underline{T}^{d}\, d\nu^{e} \right) \tag{23}$$

and the vector of plastic forces associated to each phase:

$$\underline{F}_p^m = \sum \int_{v^e} {}^t\mathbf{B}_e \cdot \mathbf{d}^m \cdot \underline{\varepsilon}_p^m dv^e \tag{24}$$

$$\underline{F}_p^r = \sum \int_{v^e} \sum_{r=1}^{N} a^r \varepsilon_p^r {}^t\mathbf{B}_e \cdot \underline{\mathbf{e}}_\mathbf{r} dv^e \tag{25}$$

### 3.2 Plastic integration algorithm

Due to the non-linearity of the phases constitutive laws, the loading path is divided into load increments noted by $\underline{\Delta F}_j^{\text{ext}}$. For each load step, the problem is solved by an iterative algorithm.

Denoting by $\left\{\underline{U}_n, \underline{\underline{\sigma}}_n^m, \sigma_n^r, \underline{\underline{\varepsilon}}_n, \underline{\underline{\varepsilon}}_{p,n}^m, \varepsilon_{p,n}^r\right\}$ the set of state variables describing the system after load step $n$. For each variable $\chi$ in this set, let us write:

$$\Delta\chi_n = \chi_{n+1} - \chi_n \tag{26}$$

Let us apply the load increment $\underline{\Delta F}_j^{\text{ext}}$. The corresponding displacements increment $\underline{\Delta U}_n$ is obtained from the global equilibrium.

$$\mathbf{K} \cdot \underline{\Delta U}_n = \underline{\Delta F}_n^{ext} + \underline{\Delta F}_{p,n} \tag{27}$$

where $\underline{\Delta F}_{p,n} = \underline{\Delta F}_{p,n}^m + \underline{\Delta F}_{p,n}^r$ is the vector of plastic nodal forces. These forces are unknown, since the plastic strain increments $\left\{\underline{\underline{\varepsilon}}_{p,n}^m, \varepsilon_{p,n}^r\right\}$ resulting from the load increment $\underline{\Delta F}_n^{\text{ext}}$ are still unknown. The latter have to be determined in such a way that the elastoplastic constitutive laws are satisfied in each Gauss point of the mesh.

The goal is achieved by using an iterative procedure. Starting from: $\underline{\underline{\Delta\varepsilon}}_{p,n}^m(0) = \Delta\varepsilon_{p,n}^r(0) = 0$ at every Gauss point, sucessive evalutions $\left\{\underline{\underline{\varepsilon}}_{p,n}^m(i), \varepsilon_{p,n}^r(i)\right\}$ of the plastic strains are calculated until convergence.

Suppose that $\left\{\underline{\underline{\varepsilon}}_{p,n}^m(i-1), \varepsilon_{p,n}^r(i-1)\right\}$ is known at each Gauss point, the vector of plastic forces calculated by (34) and (35) being $\underline{\Delta F}_{p,n}^m(i-1)$ and $\underline{\Delta F}_{p,n}^r(i-1)$. The iteration $i$ consists first in computing the increment of nodal displacement $\underline{\Delta U}_n(i)$ satisfying:

$$\mathbf{K} \cdot \underline{\Delta U}_n(i) = \underline{\Delta F}_n^{ext} + \underline{\Delta F}_{p,n}(i-1) \tag{28}$$

Following the global calculation yielding the displacement vector $\underline{\Delta U}_n(i)$, the constitutive laws have been checked locally in each Gauss point. The original point of the present implementation is the separate treatment of each individual phase. The power of the multiphase approach is thus totally exploited. The classical return mapping algorithm, Simo and Hughes (1998), is applied in each Gauss point as follows:

At first, trial stress states are calculated for each phase by freezing the plastic strains resulting from the load increment. Then the phase yield criteria are evaluated separately. If they are negative, no additional plastic strain has developed due to $\underline{\Delta F}_n^{\text{ext}}$. If not, a closest-point projection of the trial states onto their respective yield surfaces is performed.

For the matrix phase, this leads to solving the following set of equations:

$$f^m\left(\underline{\underline{\sigma}}^{n+1}(i)\right)=0 \tag{29}$$

$$\underline{\underline{\sigma}}^{n+1}(i)=\underline{\underline{\sigma}}^{trial,m}_{n+1}(i)-\underline{\underline{a}}^{m}:\underline{\underline{\Delta\varepsilon}}^{m}_{p,n}(i) \tag{30}$$

$$\underline{\underline{\Delta\varepsilon}}^{m}_{p,n}(i)=\Delta w_i\left(\frac{\partial g^m}{\partial \underline{\underline{\sigma}}^{m}}\right) \tag{31}$$

Considering now the reinforcement phase, the yield criterion can be written as $f^r(\sigma^r)=\left|\sigma^r\right|-\sigma^r_o$ due to the one-dimensional formulation. The solution for the projection problem and the related plastic strain increment is:

$$\sigma^r_{n+1}(i)=\begin{cases}\sigma^r_o & \text{se } \underline{\underline{\sigma}}^{trial,r}_{n+1}(i)\geq\sigma^r_o\\ -\sigma^r_o & \text{se } \underline{\underline{\sigma}}^{trial,r}_{n+1}(i)\leq-\sigma^r_o\end{cases} \tag{32}$$

$$\Delta\varepsilon^r_{p,n}(i)=\frac{\sigma^{trial,r}_{n+1}(i)-\sigma^r_{n+1}(i)}{a^r} \tag{33}$$

### 3.3 Failure criterion

The strength of concrete under multiaxial states of stress may be estimated from the so-called Ottosen failure criterion given by Equation 34 (CEB, 1990).

$$\alpha\frac{J_2}{f^2_{cm}}+\lambda\frac{\sqrt{J_2}}{f_{cm}}+\beta\frac{I_1}{f_{cm}}-1=0 \tag{34}$$

where $\lambda$, $J_2$, $I_1$ depend on the principal stresses and $\alpha$ and $\beta$ are material properties which depend on the strength ratio $f_{ctm}/f_{cm}$ (tensile and compression concrete strength).

### 3.4 Stress-strain relationship for concrete under compression

A uniaxial stress-strain relationship for compressed concrete is assumed as hardening rule. This stress-strain diagram has the form shown schematically in Figure 3 and is calculated by the following function (CEB, 1990):

$$\sigma_c=-\frac{\frac{E_{ci}}{E_{c1}}\frac{\varepsilon_c}{\varepsilon_{c1}}-\left(\frac{\varepsilon_c}{\varepsilon_{c1}}\right)^2}{1+\left(\frac{E_{ci}}{E_{c1}}-2\right)\frac{\varepsilon_c}{\varepsilon_{c1}}}f_{cm} \tag{35}$$

where $E_{ci}$ is the concrete tangent modulus, $E_{ci}$ = - $f_{cm}$/0,0022, $\sigma_c$ is the strength compressive stress (MPa), $\varepsilon_c$ is the compression strain and $\varepsilon_{c1}$ = -0.0022.

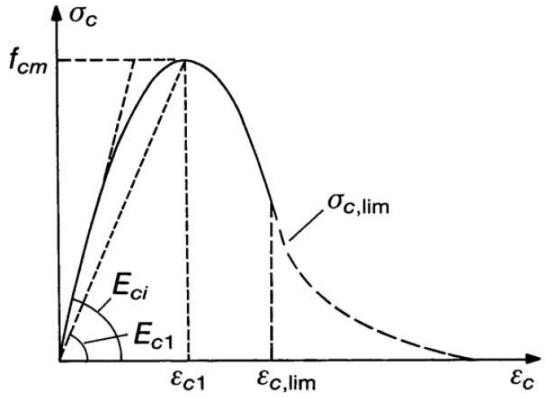


Figure 3 – Stress-strain diagram for uniaxial compression.

### 3.5 Modeling of cracked concrete (Hinton, 1988)

Probably the main feature of plain concrete material behavior is its low tensile strength, which results in tensile cracking at very low stress compared with the failure stress in compression. In the finite element context two main approaches have been used for crack representation, the *discrete crack model* that represents the individual cracks as actual discontinuities in the finite element mesh; the *smeared crack model* in which the cracked concrete is assumed to remain a continuum and the material properties are modified to account for damage. The second alternative will be adopted in this work.

### 3.6 The smeared crack model

The concrete is initially isotropic, but cracking induces anisotropy. After cracking, the concrete is assumed to become orthotropic, with the principal material axes oriented along the directions of cracking. The material properties depend on the state of strain and stress. The Young's modulus is reduced in the direction perpendicular to the crack plane and Poisson's effect is usually neglected. This approach is computationally attractive, since the topology of the mesh is unchanged throughout the analysis, and only the stress-strain relationship need to be updated when cracking occurs. In order to implement the smeared crack model, the following items have to be applied: a cracking criterion, a strain-softening rule and a model for shear transfer.

Due to bond forces, cracked concrete carries between the cracks a certain amount of tensile stress normal to the cracked plane. The concrete adheres to reinforcing bars and contributes actively to the overall stiffness of the structure. This can be incorporated into the computational model assuming that the loss of tensile strength in concrete occurs gradually and such procedure has been extensively used in computational analysis of reinforced concrete structures. According to Hinton (1988) it is easy to choose a tension-stiffening curve that will adequately fit experimental results, but very difficult to make an *a priori* predictions.

For the tensile concrete it will be used the constitutive equation (Eq. 36) adopted by Prates Junior (1992), Martinelli (2003) and other authors

$$\sigma_i = \alpha_t f_{ci}\left(1 - \frac{\varepsilon_{ui}}{0{,}01}\right) \tag{36}$$

where $\alpha_t$ is the reduction coefficient related to cracking strength and, $\sigma_i$ and $\varepsilon_{ui}$ respectively denote the stress and strain component following principal direction $i$. The following curve explain this relationship.

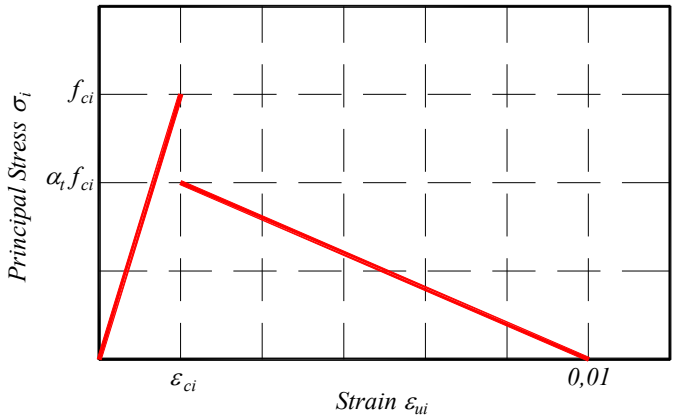


Figure 4 – Stress-strain curve for concrete under tensile load.

## 4 APPLICATIONS

The following numerical examples were performed in order to verify the proposed element model and formulation in this paper.

### 4.1 McNeice's corner-supported reinforced concrete slab with a point load

The results of a corner-supported two-way square reinforced concrete slab, tested experimentally under a central point load by Jofriet and McNeice (1971), have been used as a benchmark for verification of numerical schemes by several researchers (Zhang *et al*, 2007), and this slab was analyzed using the multiphase model to assess the accuracy and performance of the proposed schemes for RC slabs. The geometry and reinforcement of the slab are shown in Figure 5 and the material properties are those of Table 1.

| Phase | Properties | |
|---|---|---|
| Matrix (concrete) | Young's modulus | 28600 MPa |
| | Poisson's ratio | 0,15 |
| | Compression strength | 38 MPa |
| | Tensile strength | 3,8 MPa |
| | $\alpha_t$ reduction coefficient | 0,4 |
| Reinforcement (steel) | Young's modulus | 200000 MPa |
| | Yield stress | 350 MPa |

Table 1: Material properties.

The finite element mesh used to perform the simulations consists in two hundred twenty-noded hexahedral elements. The cross-section of the slab was divided into eight concrete layers and one or more equivalent steel layers with reinforcement in two directions, with one

quarter of the slab being analyzed owing to symmetry with a 5 x 5 meshing of the quadrant (Figure 5).

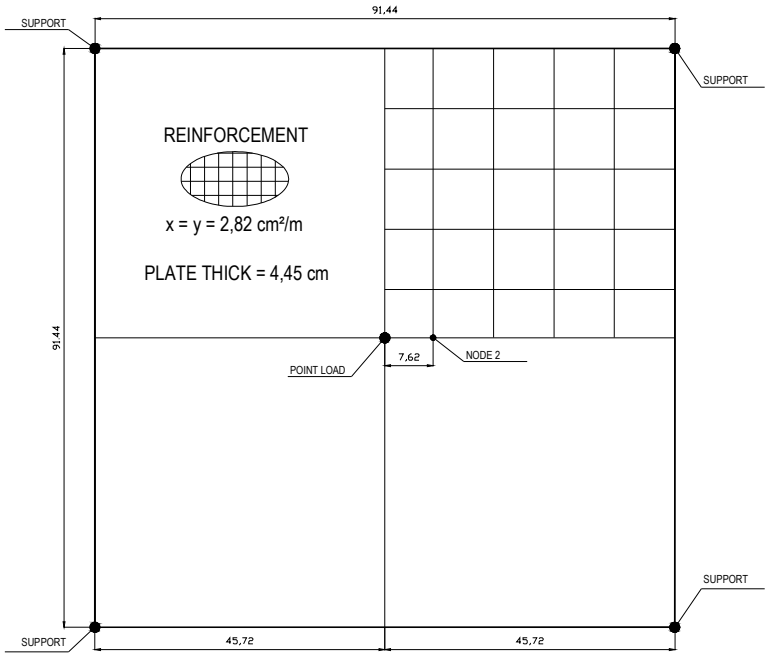


Figure 5 – Geometry of the reinforced concrete slab.

The slab is reinforced by a distribution of parallel steel bars introduced following directions $e_x$ and $e_y$. The loading mode corresponds to a bending-like test with just one point loaded.

Numerical simulations are performed corresponding to five different reinforcement distributions along the transversal section. Example 0 has no reinforcement while Example 1 has the reinforcements distributed all along the cross-section. Examples 2, 3 and 4 have the steel distributed at the inferior region of the structural element as it can be seen in Figure 6. It is very important to point out that variable called volumetric fraction $\eta$, varies in each model aiming to maintain the same amount of steel reinforcement.

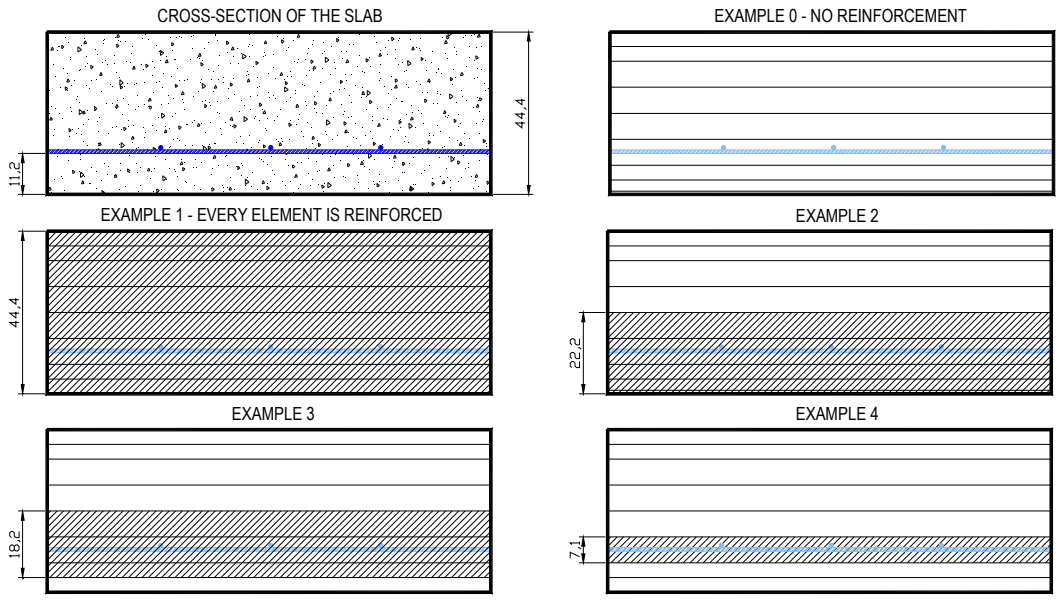


Figure 6 – Reinforcement scheme: the hatched regions indicating reinforced layers.

Figure 7 presents the numerical and experimental results. It has been found from the comparisons that the numerical results agree with the experimental tests. Obviously Example 1 gave the worst result since the center of mass of the steel bars wasn't observed. The influence of the area where the reinforcement is applied is reported in Figure 8.

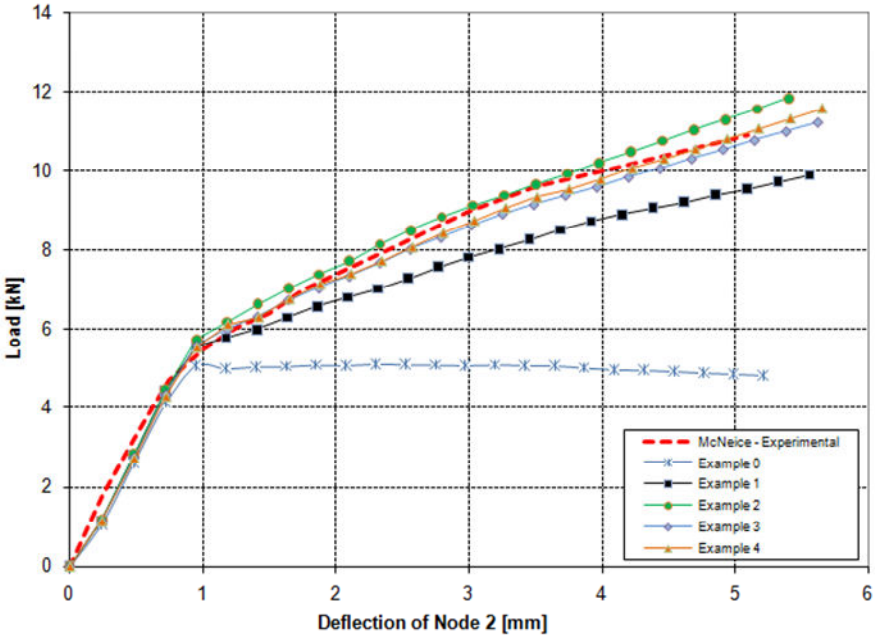


Figure 7 – Load-deflection curves at node 2 of McNeice's slab under a central point load.

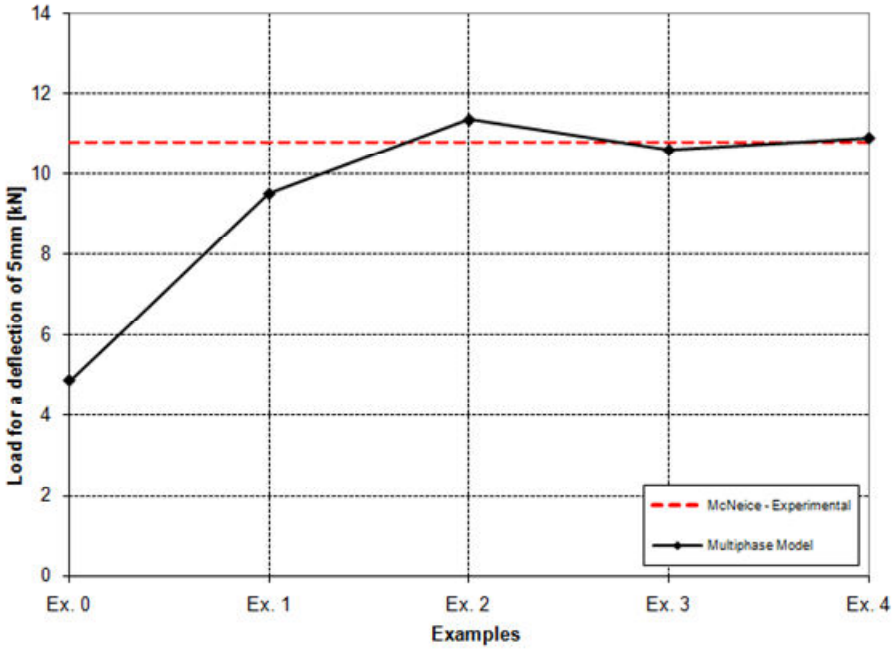


Figure 8 – Load for a deflection of 5mm at node 2.

An important issue of the computational modeling is to determine the extent of the multiphase zone (i.e., reinforced zone). Actually, this aspect is related to the validity of the

approach, since the later theoretically requires that the density of reinforcement is much higher for the material to be regarded at the macroscopic scale as an 'homogeneous' two phase material.

The analysis indicates that the configurations of Example 3 and 4 converge to the experimental result meaning that, for the adopted example, reinforced zone with extension of 40,9% (1,82cm/4,44cm) and 15,9% (0,71cm/4,44cm) prove to be enough for an appropriate representation of the reinforced zone. This results is still to be confirmed by further investigations.

## 5 CONCLUDING REMARKS

A multiphase model for structures of reinforced concrete with perfect bounding between the steel bars and the matrix of concrete and considering the concrete cracking was introduced. The implementation and validation of this model is the object of the doctorate thesis of the first author. The comparative study performed with McNeice's reinforced concrete slabs produced results in good agreement with the experimental results. In terms of future development, the model will be extended to include more realistic conditions than perfect bonding, allowing some kind of sliding between the matrix phase and the reinforcement phase.

## ACKNOWLEDGEMENTS

Finally, my thanks to CNPq (Brazilian National Council for Scientific and Technological Development) for financial support which enabled this work.

## REFERENCES

BENNIS, M. Un modèle multiphasique pour le calcul des ouvrages renforcés par inclusions, avec prise en compte de l'interaction matrice/inclusions. *Thèse de doctorat de l'École Nationale des Ponts et Chaussés*, Paris, 2002.

de BUHAN, P., SUDRET, B. A two-phase elastoplastic model for unidirectionally-reinforced materials. *European Journal of Mechanics A/Solids*. 1999, pp 995-1012.

de BUHAN, P., SUDRET, B. Micropolar multiphase model for materials reinforced by linear inclusions. *European Journal of Mechanics A/Solids*. 2000, pp 669-687.

de BUHAN, P., SUDRET, B. Multiphase model for inclusion-reinforced geostructures Application to rock-bolted tunnels and piled raft foundations. *International Journal for numerical and analytical methods in geomechanics*. 2001, pp 155-182.

COMITÉ EURO-INTERNATIONAL DU BÉTON (CEB). "Application of the Finite Element-Method to Two-Dimensional Reinforced Concrete Structures". Paris, 1983. (Bulletin d'Information, 159).

FIGUEIREDO, M. P., MAGHOUS, S., CAMPOS FILHO, A. Elastoplastic multiphase model for reinforced concrete flat slabs. CILAMCE, 2009.

HASSEN, G. Modélisation multiphasique pour le calcul des ouvrages renforcés par inclusion rigides. *Thèse de doctorat de l'École Nationale des Ponts et Chaussés*, Paris, 2006.

HASSEN, G., de BUHAN, P. A two-phase model and related numerical tool for the design of soil structures reinforced by stiff linear inclusions. *European Journal of Mechanics A/Solids*. 2005, pp 987-1001.

HASSEN, G., de BUHAN, P. Elastoplastic multiphase model for simulating the response of piled raft foundations subject to combined loadings. *International Journal for numerical and analytical methods in geomechanics*. 2006, pp 843-864.

HINTON, E. Numerical methods and software for dynamic analysis of plates and shells. Swansea: Pineridge Press, 1988.

JOFRIET, J. C., McNEICE, G. M. Finite-element analysis of reinforced concrete slabs, *J. Struct. Div*. ASCE 97 (ST3), 1971, pp. 785-806.

SIMO, J. C., HUGHES, T. J. R. Computational Inelasticity. *Springer,* Berlin, 1998.

SUDRET, B. Modélisation multiphasique des ouvrages renforcés par inclusions. *Thèse de doctorat de l'École Nationale des Ponts et Chaussés*, Paris, 1999.

ZHANG, Y. X., BRADFORD, M. A., GILBERT, R. I. A layered shear-flexural plate/shell element using Timoshenko functions for nonlinear analysis of reinforced concrete plates. *Finite Elements in Analysis and Design 43*, 2007, pp. 888–900.